

Topological Superconductivity in Rashba Spin-Orbital Coupling Suppressed Monolayer β -Bi₂Pd

Xin-Hai Tu,^{1,2,3} Peng-Fei Liu,^{1,3} Wen Yin,^{1,2,3} Jun-Rong Zhang,^{1,2,3} Ping Zhang,^{4,5} and Bao-Tian Wang^{1,2,3,6,*}

¹*Institute of High Energy Physics, Chinese Academy of Sciences (CAS), Beijing 100049, China*

²*University of Chinese Academy of Sciences, Beijing 100039, China*

³*Spallation Neutron Source Science Center, Dongguan 523803, China*

⁴*School of Physics and Physical Engineering, Qufu Normal University, Qufu 273165, China*

⁵*Institute of Applied Physics and Computational Mathematics, Beijing 100088, China*

⁶*Collaborative Innovation Center of Extreme Optics, Shanxi University, Taiyuan, Shanxi 030006, China*

(Dated: March 13, 2024)

The weak interlayer Van Der Waals material β -Bi₂Pd has recently been established as a strong topological superconductor candidate with unconventional spin-triplet pairing and Majorana zero modes at vortices. In this letter, we study the topological characters and the superconducting pairing, which are still obscure in monolayer β -Bi₂Pd, in light of our effective theoretical model. We find that the non-Rashba spin-orbital coupling plays a critical role in realizing and tuning various novel topological natures. In particular, the spin-triplet p-wave superconducting pairing with Majorana zero mode is revealed in monolayer β -Bi₂Pd. Our studies deepen the understanding of topology and superconductivity in monolayer β -Bi₂Pd and indicate it is a promising platform for achieving low-dimensional topological superconductivity.

Introduction Since Majorana Fermions are their own antiparticles and obey non-Abelian braiding statistics [1, 2], they possess potential applications for fault-tolerant topological quantum computation [3–5]. Topological superconductor (TSC) [6–8] with unconventional pairing symmetry is a natural platform for realizing topologically protected gapless boundary states which is essentially Andreev bound state hosting Majorana fermions [9, 10]. The p-wave superconductor Sr₂RuO₄ [11–13] is a chiral TSC associated with spontaneous time-reversal (TR) symmetry breaking. Cu-doped Bi₂Se₃ [14, 15], an odd-parity superconductor [16, 17], is judged as the TR invariant TSC from the Fermi surface of normal state that encloses an odd number of time-reversal invariant momenta in the first Brillouin zone (BZ) [18–20]. In addition, a feasible project is proposed [21] to support non-Abelian anyon excitations, which is realized in two-dimensional (2D) Dirac Fermions, in s-wave superconductors. Subsequently, it is explicitly demonstrated by both theory [22] and experiment [23–25] that the Dirac-type surface state from a topological insulator couplings to a s-wave superconductor resembles a spinless p-wave superconductor where Majorana zero modes (MZMs) are realized at vortices.

Recently, a promising TSC candidate β -Bi₂Pd has attracted much attention on its topologically protected surface state [26–28] and fully-gapped anisotropic s-wave superconductivity [29, 30]. The angle-resolved photoemission spectroscopy measurements on β -Bi₂Pd thin films show an anomalously large superconducting gap of topological surface state [31]. Furthermore, a signature of MZMs at vortices was observed via cryogenic scanning tunneling microscopy [32]. Much interest is sparked by the observation of half-quantum magnetic flux quantization indicating an unconventional superconductor with the spin-triplet pairing symmetry [33]. Besides the bulk structure, fertile ground in monolayer β -Bi₂Pd is still uncultivated and worth equal studying owing to its manipulatable property and abundant topological physics inside.

In this letter, we are motivated to understand the topolog-

ical and superconducting properties in monolayer β -Bi₂Pd. The bulk β -Bi₂Pd is a layered structure with tetragonal centrosymmetric space group I4/mmm as shown in Fig. 1 (a) which is drawn by VESTA [34]. Using molecular beam epitaxy method, the monolayer structure could be synthesized in experiment [35]. Our optimized lattice constant is $a = 3.322$ Å, which is slightly smaller than the experimental value 3.4 Å of the β -Bi₂Pd films [32]. Based on the reduced three-band tight-binding model (TBM), the complete process of topological phase transition is displayed by tuning spin-orbital coupling (SOC). Here, the Rashba SOC is suppressed. On the one hand, we find that the high-order quadratic Dirac point (DP) protected by C₄ rotation symmetry appears at the M point when ignoring the effect of SOC. On the other hand, including SOC, quantum spin Hall phase with nontrivial topological edge states (TESSs) begin to emerge if the strength of SOC is less than 6.39 eV. The nontrivial phase is characterized by the spin Chern number (SCN) $C_s = 1$. In addition, we study pairing symmetry around the M point as well as the corresponding linearized gap equations, since monolayer β -Bi₂Pd is a superconductor according to first-principles calculations [36]. Specifically, we find that monolayer β -Bi₂Pd is a Dirac superconductor with p-wave superconducting pairing when excluding SOC. Including SOC, it becomes a TSC of symmetry class D with MZMs at the boundary. The details of computation is shown in supplementary information (SI).

Basis and Model Hamiltonian In order to get a physics picture of monolayer β -Bi₂Pd, we begin to choose suitable atomic orbitals. We find that the p -orbitals of Bi atoms contribute mainly to the band structure around the Fermi level through the whole BZ, while the d -orbitals of Pd atoms are away from p -orbitals and only dominant on the valence bands from -5 to -2 eV, as shown in Fig. 2 (a). Meanwhile, the bands below -6 eV are disentangled with the above. Thus, we fit a eleven-band TBM by Wannier90 package [37] first, which reproduce the bands around the Fermi level [red lines in Fig. 2 (b)]. Then, to simplify the problem, we treat the

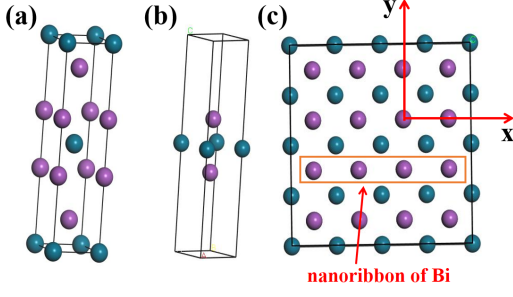


FIG. 1. The bulk (a) and monolayer structure (b) of β -Bi₂Pd. The purple balls are Bi atoms, and navy blue balls are Pd atoms. (c) The top view of monolayer β -Bi₂Pd.

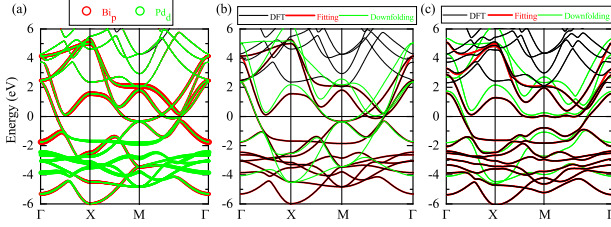


FIG. 2. The band structure of monolayer β -Bi₂Pd without (a) (b) and with (c) SOC. The contribution of p_z and $p_{x,y}$ orbitals of Bi atoms is signed by red and green balls. The red lines represent the fitting eleven bands drawn according to wannier90. The green lines represent downfolding six bands.

influence of Pd atoms as the perturbation and get a six-band TBM upto the fourth-nearest-neighbor hopping by downfolding technique [38–40] (see SI). Since the existence of inversion symmetry, it is natural to set up bonding and anti-bonding states with definite parity [41] for Bi atoms as follow:

$$|\text{Bi}_{x,y,z}^{\pm}\rangle = \frac{1}{\sqrt{2}}(|\text{Bi}_{1;x,y,z}\rangle \mp |\text{Bi}_{2;x,y,z}\rangle), \quad (1)$$

where the superscript represents the parity. Eventually, we get a block diagonal six-band TBM (shown in SI). The fitting parameters are shown in Table S1. One can see that the contribution of Pd atoms does not introduce any additional hopping terms. In other words, in our case, we could equivalently only take Bi atoms into account to construct TBM and ignore the influence from the ineffective Pd atoms. One of the main reasons is that Bi and Pd atoms have the same site symmetry (4mm).

Spin-orbital Coupling Owing to the heavy halogen family Bi, we consider the SOC effect in our model. Since potential field is the largest near the atomic nuclei, SOC is normally accurately approximated by a local atomic contribution of the form

$$H_{\text{SOC}} = \frac{dV(\mathbf{r}_i \times \mathbf{p}_i) \cdot \mathbf{S}_i}{dr \cdot 2r(mc)^2} = 2\lambda \mathbf{L}_i \cdot \mathbf{S}_i, \quad (2)$$

where $\lambda = 0.578$ eV and denotes the strength of SOC, \mathbf{L}_i and \mathbf{S}_i are orbital and spin angular momentum on site i of electron,

respectively. Since the coincidence of TR and inversion symmetry, the Kramer degeneracy ensures the double degeneracy of each band. Therefore, it is no accident that SOC is nothing but splits the DP at the M point and causes a full band gap as shown in Fig. 2(c). Here, we ignore the SOC effect of Pd atoms which is much smaller than Bi ($\lambda_{\text{Pd}} = 0.087$ eV). The in-plane SOC effect (Rashba SOC) coupling bands between bonding and anti-bonding states is excluded from consideration as well. Experimentally, it could be tunable by the electric field along z direction. So, we get the full Hamiltonian with SOC (see SI). In the case, the Hamiltonian is still block diagonal, which means that the spin z component is not mixed and hence is still a good quantum number. Next, we focus on H_{S1} that we are interested and won't go into details about H_{S2} since H_{S1} is independence of H_{S2} .

High-Order Dirac Point Without SOC, there is a distinct DP [42–44] at the M point which is protected by C_4 rotation symmetry and is robust against any perturbations unless destroying the crystal symmetry. To illustrate the topological properties of the DP, we drop off the p_z orbital and reduce the TBM H_{S1} into the 2×2 continuum model around the M point using perturbation theory, since the p_z orbital is far away from the other two orbitals [45]. In this case, the kernel of the Hamiltonian is still grasped from such virtual process in which a electron jumps from the $p_{x,y}$ to the p_z orbital and then back to $p_{x,y}$ orbitals. Thus, the continuum Hamiltonian expanding at the M point reads (keep to the lowest terms of \mathbf{k})

$$H_M = m_3 k_x k_y \sigma_x + \lambda \sigma_y + \frac{m_1 - m_2}{2} (k_x^2 - k_y^2) \sigma_z, \quad (3)$$

where σ is the Pauli matrix on the orbital space. Next, we define a 2D planar vector \mathbf{d} (see SI), which has a vortex structure at the DP ($\lambda = 0$) from Fig. S2. This vortex is described by the winding number

$$W = \oint_C \frac{d\mathbf{k}}{2\pi} \cdot \left(\frac{d_x}{|\mathbf{d}|} \nabla \frac{d_y}{|\mathbf{d}|} - \frac{d_y}{|\mathbf{d}|} \nabla \frac{d_x}{|\mathbf{d}|} \right), \quad (4)$$

which is 2 in our present case. Thus, the DP is a high-order DP with quadratic dispersions [46, 47]. One can find more details about the continuum model in SI.

Topological phase transition By adiabatic continuity, as long as the Hamiltonian is gapped, it remains in the same topological phase (TP) unless it encounters gapless points which are TP transition points (TPTPs). The DP we mentioned before is exactly the TPTP connecting two different TPs. In fact, with the change of λ , the conduction and valence bands also close at another critical point Γ [Fig. S1 (b)] when $\lambda_0 = 6.39$ eV. Then we can write down the continuum model at the Γ right now (upto the leading order)

$$H_{\Gamma} = \gamma_0 \sigma_0 - \gamma_1 k_y \sigma_x + \gamma_1 k_x \sigma_y + \gamma_2 \sigma_z. \quad (5)$$

Next, we show different topological phases as λ goes from large to small [7]. First of all, when λ is extremely large upto infinity ($+\infty$), the Hamiltonian is topologically equivalent to the atomic limit, due to the flat and \mathbf{k} -independent band structures. However, things start to change when we go through the

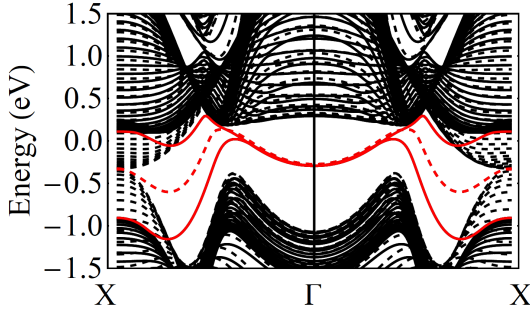


FIG. 3. The projected band structures along [01] direction with (solid lines) and without (dashed lines) SOC. TESSs are marked with red lines.

first critical point Γ . The difference of SCN between $\lambda > \lambda_0$ and $0 < \lambda < \lambda_0$ is -1, so SCN of the phase is nontrivial and given by $C_s = -1$. If we decrease λ to zero, we reach another critical point M. The change of SCN is 2, thus the new phase has a nontrivial SCN $C_s = 1$. Finally, the Hamiltonian is back to the trivial state when $\lambda < -\lambda_0$ which is the same as the case $\lambda > \lambda_0$. SCN is calculated by integral Berry curvature $F(\mathbf{k}) = i\nabla u(\mathbf{k}) \times \nabla v(\mathbf{k})$ over the whole BZ as follow [48, 49]

$$C_s = \frac{1}{2\pi} \int d^2k F(\mathbf{k}), \quad (6)$$

where $u(\mathbf{k})$ is the wavefunction. Around the TPTs Γ and M, SCN is given by $C_s = \frac{1}{2}\text{sgn}(\eta)$ and $C_s = \text{sgn}[\lambda m_3(m_1 - m_2)]$, respectively, where $\eta = \pm 1$. Meanwhile, the existence of inversion symmetry helps us to describe the nontrivial TP by \mathcal{Z}_2 index via parity method [50, 51] as shown in Table S2. There is a distinct band inversion along Γ -X line that results in nontrivial $\mathcal{Z}_2 = 1$.

Topological Edge State Besides SCN, another remarkable feature of a nontrivial topological phase is topological boundary state. Considering an infinite nanoribbon of monolayer β -Bi₂Pd where y direction is limited (Fig. 1), in the case, the momentum component k_y is not a good quantum number yet. In Fig. 3, we plot the projected edge band structure of nontrivial TP for H_{S1} . Excluding SOC, we can see a TES connects two projected DPs as in graphene model [52]. Once turning on SOC, the band structure in bulk will be divided and then forms a full band gap. However, the TESs close the band gap at the Γ point (solid red lines). The TESs corresponding to quantum spin Hall state [52, 53] that two electrons with opposite spin travel toward adverse directions at the boundary since the system preserves the TR symmetry. To show the validity of our model further, in Fig. S3, we show the Bi terminated TESs calculated by WannierTools package [54] as a control, whose main physical features are captured in our effective six-band model.

Pairing Symmetry and Majorana Zero Mode Below the superconducting transition temperature (STT) $T_c = 1.95$ K [36], Cooper pairs are formed from two electrons occupying orbitals of $|\text{Bi}_{x,y}^\pm\rangle$. According to U-V model [9, 20], we classify all possible on-site and nearest neighbor superconduct-

TABLE I. Classification of all on-site and nearest neighbor pairing potentials according to the representations of D_{4h} point group.

| Form factors | Representation | Matrix form | Spin |
|--|---|--------------------------------|---------|
| $A_{1g}/B_{1g}, \cos(kx) \pm \cos(ky)$ | $A_{1g}, \Delta_{\alpha 1}$ | $\sigma_0 s_0$ | Singlet |
| | $A_{1g}, \Delta_{\alpha 2}$ | $\sigma_y s_z$ | Triplet |
| | $B_{1g}, \Delta_{\alpha 3}$ | $\sigma_z s_0$ | Singlet |
| | $B_{2g}, \Delta_{\alpha 4}$ | $\sigma_x s_0$ | Singlet |
| | $E_g, (\Delta_{\alpha 5}, \Delta_{\alpha 6})$ | $(\sigma_y s_x, \sigma_y s_y)$ | Triplet |
| $E_u, [\sin(kx), \sin(ky)]$ | E_g | $(\sigma_0 s_x, \sigma_0 s_y)$ | Triplet |
| | E_g | $(\sigma_z s_x, \sigma_z s_y)$ | Triplet |

ing pairing potentials $\Delta_{\alpha i}(\mathbf{k}) = \Delta_0 f_{\alpha}(\mathbf{k}) \Gamma_i$ under the constraint of point group D_{4h} in Table I, where U and V are intraorbital and interorbital interactions, respectively, α is pairing symmetry index, $f_{\alpha}(\mathbf{k})$ is pairing form factor, and Γ_i is the i^{th} matrix form of irreducible representation of pairing potentials. For p-wave superconducting states, we consider the states with TR and C_4 rotation symmetry. Thus, only two odd-parity pairings survive: $\Delta_{p1}(\mathbf{k}) = \sin k_x \sigma_z s_x + \sin k_y \sigma_0 s_y$ and $\Delta_{p2}(\mathbf{k}) = \sin k_x \sigma_z s_x - \sin k_y \sigma_z s_y$ (note that these components $\sin(k_x/k_y) \sigma_0/z s_x \pm \sin(k_y/k_x) \sigma_0/z s_y$ are equivalent). Both of them are belong to the representation A_{1u} . On the Nambu basis $\{C_{\mathbf{k}z,\uparrow}^\dagger, C_{\mathbf{k}x,\uparrow}^\dagger, C_{\mathbf{k}y,\uparrow}^\dagger, C_{\mathbf{k}z,\downarrow}^\dagger, C_{\mathbf{k}x,\downarrow}^\dagger, C_{\mathbf{k}y,\downarrow}^\dagger, C_{-\mathbf{k}z,\downarrow}, C_{-\mathbf{k}x,\downarrow}, C_{-\mathbf{k}y,\downarrow}, -C_{-\mathbf{k}z,\uparrow}, -C_{-\mathbf{k}x,\uparrow}, -C_{-\mathbf{k}y,\uparrow}\}$, the Bogoliubov-de Gennes (BdG) Hamiltonian for H_{S1} is given by

$$H_{BdG1} = \begin{bmatrix} H_{S1}(\mathbf{k}) & \Delta_{\alpha i} \\ \Delta_{\alpha i}^\dagger & -s_y H_{S1}^*(-\mathbf{k}) s_y \end{bmatrix}. \quad (7)$$

In Figs. S4-S7, we show the superconducting band structures for different pairing potentials. For s-wave pairing without SOC, the spin-singlet pairing Δ_{s1} gives a full superconducting gap. Nevertheless, when monolayer β -Bi₂Pd enters Δ_{s2} phase, it becomes a nodal loop superconductor where the loop surrounds the M point which is the same as Δ_{s5} (Δ_{s5} is equivalent to Δ_{s6}). For Δ_{s3} (Δ_{s4}) pairing, the DP appears on the M- Γ (X-M) line. Once turning on SOC, pairings Δ_{s2} will open a superconducting band gap. If SOC strength is larger than the gap function strength $|\lambda| > |\Delta_0|$, $\Delta_{s3/4/5}$ will be gapped as well. For s*-wave, it is the same as s-wave. However, for d-wave pairing, due to the form factor of $f_d(\mathbf{k}) = \cos k_x - \cos k_y$, there are always DPs along M- Γ line for all channels without SOC. With SOC, if $|\lambda|$ is larger enough, the superconducting gaps will appear. For p-wave, Δ_{p1} give a superconducting band gap but Δ_{p2} has a Dirac point along M- Γ line without SOC. With SOC, these two pairings are gapped.

The continuum model at the M point is illustrative of issues. Here, we take pairing potential Δ_{s2} as an example. The superconducting eigenvalue is given in SI. One can see when λ is zero, a Fermi loop around the M point is obtained by solving such \mathbf{k} -equation $[\frac{(m_1 - m_2)}{2}(k_x^2 - k_y^2)]^2 + (m_3 k_x k_y)^2 = \Delta_0^2$. The diagrammatic sketch is shown in Fig. S8 (a) in which the loop is actually a rounded square. More details of other pairings are shown in SI.

Next to determine the possible superconducting pairings,

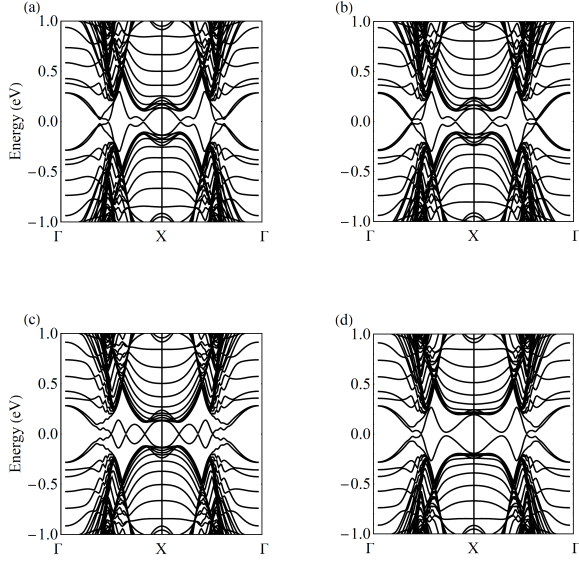


FIG. 4. The Majorana Zero modes for different pairing potentials (a) Δ_{d1} , (b) Δ_{d2} , (c) Δ_{p1} , (d) Δ_{p2} . Here, we set $\lambda = 0.578$ eV and $\Delta_0 = 0.3$ eV as examples.

we evaluate the linearized gap equations in each pairing potential (see SI). In the strong SOC limit ($\lambda \approx \mu$), the possible channel in s-wave pairing is A_{1g} which gives the STT by $k_B T_c = \frac{2e^\gamma}{\pi} \omega_D \exp\left(-\frac{1}{2g(0)V_{eff}}\right)$. Here, μ is the chemical potential, ω_D is the Debye frequency, $\gamma \approx 0.5772$ is the Euler constant and $g(0)$ is the density of states at the Fermi level. The effective interaction $V_{eff} = U + V \frac{\lambda^2}{\mu^2} \approx U + V$. For non-on-site pairing, rather than performing an accurate calculation of STT [55–57], we qualitative evaluate the relative relation of STT in each channel. The possible pairings for s*-wave and d-wave are the same as s-wave. For p-wave pairing, Δ_{p1} has a vanishing STT and the possible superconducting ground state is Δ_{p2} . In Fig. 4, we show TESs for these possible superconducting pairings in which $\Delta_{d/p}$ has nontrivial MZM. It is proved that two copies of the chiral spinless p-wave superconductor is a intrinsic TR invariant TSC [8]. As shown in Fig. S9, even if SOC is excluding, MZM still survives in pairing Δ_{p1} . In view of the experimental observation of the spin-triplet p-wave superconducting pairing [33], Δ_{p2} is considered to be a strong pairing candidate in monolayer β -Bi₂Pd. In the case, the BdG Hamiltonian commutes with z component of spin $[H_{BdG1}, S_z] = 0$, which implies that the Hamiltonian can be brought into block-diagonal form. While these two blocks are related by TR, each block is TR breaking [58]. As a consequence, each block Hamiltonian belongs to symmetry class D and the corresponding topological invariant is \mathcal{Z} in 2D according to ten symmetry classes of topological systems [59].

Conclusion and Discussion In summary, we have presented a systematic study on topological and superconducting properties of monolayer β -Bi₂Pd. First, we show that

the effect of Pd atoms is inessential to the interested physics. The effective TBM constructed from Bi atoms can capture the main physics. Second, the previous scheme shows that Rashba SOC with Zeeman field is a possible way to realize topological superconductivity [60, 61]. Based on our model, however, we find that the non-Rashba SOC effect also plays a key role for realizing and tuning various exotic topological phenomena, such as high-order DP, quantum spin Hall state, Dirac superconducting state, nodal loop superconducting state and topological superconducting state. Finally, our results show that monolayer β -Bi₂Pd is a strong 2D TSC candidate of symmetry class D in the spin-triplet p-wave superconducting pairing channel. We hope this work could provide inspiration and guidance for further experimental and theoretical works in monolayer β -Bi₂Pd.

Acknowledgements We thank Dr. Yun-Long Lian for helpful discussions. The authors gratefully acknowledge financial support from National Natural Science Foundation of China (Grant No. 12074381) and Science Challenge Project (Grant No. TZ2016001). The authors also are thankful for the computational resources from the Supercomputer Centre of the China Spallation Neutron Source.

* Author to whom correspondence should be addressed. E-mail: wangbt@ihep.ac.cn

- [1] E. Majorana, *Il Nuovo Cimento* **14**, 171 (1937).
- [2] G. Moore and N. Read, *Nuclear Physics B* **360**, 362 (1991).
- [3] F. Wilczek, *Nature Physics* **5**, 614 (2009).
- [4] C. Beenakker, *Annual Review of Condensed Matter Physics* **4**, 113 (2013).
- [5] A. Kitaev, *Annals of Physics* **303**, 2 (2003).
- [6] X.-L. Qi, T. L. Hughes, S. Raghu, and S.-C. Zhang, *Phys. Rev. Lett.* **102**, 187001 (2009).
- [7] B. A. Bernevig and T. L. Hughes, *Topological Insulators and Topological Superconductors* (Princeton University Press, 2013).
- [8] N. Read and D. Green, *Phys. Rev. B* **61**, 10267 (2000).
- [9] M. Sato and Y. Ando, *Reports on Progress in Physics* **80**, 076501 (2017).
- [10] X.-L. Qi and S.-C. Zhang, *Rev. Mod. Phys.* **83**, 1057 (2011).
- [11] T. M. Rice and M. Sigrist, *Journal of Physics: Condensed Matter* **7**, L643 (1995).
- [12] K. Ishida, H. Mukuda, Y. Kitaoka, K. Asayama, Z. Q. Mao, Y. Mori, and Y. Maeno, *Nature* **396**, 658 (1998).
- [13] C. Kallin, *Reports on Progress in Physics* **75**, 042501 (2012).
- [14] Y. S. Hor, A. J. Williams, J. G. Checkelsky, P. Roushan, J. Seo, Q. Xu, H. W. Zandbergen, A. Yazdani, N. P. Ong, and R. J. Cava, *Phys. Rev. Lett.* **104**, 057001 (2010).
- [15] M. Kriener, K. Segawa, Z. Ren, S. Sasaki, and Y. Ando, *Phys. Rev. Lett.* **106**, 127004 (2011).
- [16] S. Sasaki, M. Kriener, K. Segawa, K. Yada, Y. Tanaka, M. Sato, and Y. Ando, *Phys. Rev. Lett.* **107**, 217001 (2011).
- [17] T. V. Bay, T. Naka, Y. K. Huang, H. Luigjes, M. S. Golden, and A. de Visser, *Phys. Rev. Lett.* **108**, 057001 (2012).
- [18] M. Sato, *Phys. Rev. B* **79**, 214526 (2009).
- [19] M. Sato, *Phys. Rev. B* **81**, 220504 (2010).
- [20] L. Fu and E. Berg, *Phys. Rev. Lett.* **105**, 097001 (2010).

- [21] M. Sato, Physics Letters B **575**, 126 (2003).
- [22] L. Fu and C. L. Kane, Phys. Rev. Lett. **100**, 096407 (2008).
- [23] P. Zhang, K. Yaji, T. Hashimoto, Y. Ota, T. Kondo, K. Okazaki, Z. Wang, J. Wen, G. D. Gu, H. Ding, and S. Shin, Science **360**, 182 (2018).
- [24] Y. Yuan, J. Pan, X. Wang, Y. Fang, C. Song, L. Wang, K. He, X. Ma, H. Zhang, F. Huang, W. Li, and Q.-K. Xue, Nature Physics **15**, 1046 (2019).
- [25] S.-Y. Guan, P.-J. Chen, M.-W. Chu, R. Sankar, F. Chou, H.-T. Jeng, C.-S. Chang, and T.-M. Chuang, Science Advances **2**, e1600894 (2016).
- [26] M. Sakano, K. Okawa, M. Kanou, H. Sanjo, T. Okuda, T. Sasagawa, and K. Ishizaka, Nature Communications **6** (2015).
- [27] T. Xu, B.-T. Wang, M. Wang, Q. Jiang, X.-P. Shen, B. Gao, M. Ye, and S. Qiao, Phys. Rev. B **100**, 161109 (2019).
- [28] B.-T. Wang and E. R. Margine, Journal of Physics: Condensed Matter **29**, 325501 (2017).
- [29] J.-J. Zheng and E. R. Margine, Phys. Rev. B **95**, 014512 (2017).
- [30] P. K. Biswas, D. G. Mazzone, R. Sibille, E. Pomjakushina, K. Conder, H. Luetkens, C. Baines, J. L. Gavilano, M. Kenzelmann, A. Amato, and E. Morenzoni, Phys. Rev. B **93**, 220504 (2016).
- [31] J.-Y. Guan, L. Kong, L.-Q. Zhou, Y.-G. Zhong, H. Li, H.-J. Liu, C.-Y. Tang, D.-Y. Yan, F.-Z. Yang, Y.-B. Huang, Y.-G. Shi, T. Qian, H.-M. Weng, Y.-J. Sun, and H. Ding, Science Bulletin **64**, 1215 (2019).
- [32] Y.-F. Lv, W.-L. Wang, Y.-M. Zhang, H. Ding, W. Li, L. Wang, K. He, C.-L. Song, X.-C. Ma, and Q.-K. Xue, Science Bulletin **62**, 852 (2017).
- [33] Y.-F. Li, X.-Y. Xu, M.-H. Lee, M.-W. Chu, and C.-L. Chien, Science **366**, 238 (2019).
- [34] K. Momma and F. Izumi, Journal of Applied Crystallography **41**, 653 (2008).
- [35] N. Denisov, A. Matetskiy, A. Tupkalo, A. Zotov, and A. Saranin, Applied Surface Science **401**, 142 (2017).
- [36] P.-F. Liu, J. Li, X.-H. Tu, H. Yin, B. Sa, J. Zhang, D. J. Singh, and B.-T. Wang, Phys. Rev. B **102**, 155406 (2020).
- [37] G. Pizzi, V. Vitale, R. Arita, S. Blügel, F. Freimuth, G. Géranton, M. Gibertini, D. Gresch, C. Johnson, T. Koretsune, J. Ibañez-Azpiroz, H. Lee, J.-M. Lihm, D. Marchand, A. Marrazzo, Y. Mokrousov, J. I. Mustafa, Y. Nohara, Y. Nomura, L. Paulatto, S. Poncé, T. Ponweiser, J. Qiao, F. Thöle, S. S. Tsirkin, M. Wierzbowska, N. Marzari, D. Vanderbilt, I. Souza, A. A. Mostofi, and J. R. Yates, Journal of Physics: Condensed Matter **32**, 165902 (2020).
- [38] P. Löwdin, The Journal of Chemical Physics **19**, 1396 (1951).
- [39] K. V. Shanavas, Z. S. Popović, and S. Satpathy, Phys. Rev. B **89**, 085130 (2014).
- [40] H.-B. Leng, C. Li, and X. Liu, Science China Physics, Mechanics & Astronomy **64**, 1869 (2021).
- [41] C.-X. Liu, X.-L. Qi, H. Zhang, X. Dai, Z. Fang, and S.-C. Zhang, Phys. Rev. B **82**, 045122 (2010).
- [42] X.-H. Tu, P.-F. Liu, and B.-T. Wang, Phys. Rev. Materials **3**, 054202 (2019).
- [43] Z. Wang, H. Weng, Q. Wu, X. Dai, and Z. Fang, Phys. Rev. B **88**, 125427 (2013).
- [44] Q. Wu, C. Piveteau, Z. Song, and O. V. Yazyev, Phys. Rev. B **98**, 081115 (2018).
- [45] K. Sun, W. V. Liu, A. Hemmerich, and S. D. Sarma, Nature Physics **8**, 67 (2011).
- [46] W. Wu, Z.-M. Yu, X. Zhou, Y. X. Zhao, and S. A. Yang, Phys. Rev. B **101**, 205134 (2020).
- [47] P.-J. Chen, W.-J. Li, and T.-K. Lee, “High-order dirac and weyl points in screw-symmetric materials,” (2020), arXiv:2009.12036.
- [48] R. Chen and B. Zhou, Physics Letters A **381**, 944 (2017).
- [49] D. N. Sheng, Z. Y. Weng, L. Sheng, and F. D. M. Haldane, Phys. Rev. Lett. **97**, 036808 (2006).
- [50] L. Fu, C. L. Kane, and E. J. Mele, Phys. Rev. Lett. **98**, 106803 (2007).
- [51] L. Fu and C. L. Kane, Phys. Rev. B **76**, 045302 (2007).
- [52] M. Ezawa, Journal of the Physical Society of Japan **84**, 121003 (2015).
- [53] X. Qian, J. Liu, L. Fu, and J. Li, Science **346**, 1344 (2014).
- [54] Q. Wu, S. Zhang, H.-F. Song, M. Troyer, and A. A. Soluyanov, **224**, 405 (2018).
- [55] K. Seo, B. A. Bernevig, and J. Hu, Phys. Rev. Lett. **101**, 206404 (2008).
- [56] C. Fang, Y.-L. Wu, R. Thomale, B. A. Bernevig, and J. Hu, Phys. Rev. X **1**, 011009 (2011).
- [57] J. Hu and H. Ding, Scientific Reports **2** (2012), 10.1038/srep00381.
- [58] Q.-Z. Wang, J. Yu, and C.-X. Liu, Phys. Rev. B **97**, 224507 (2018).
- [59] A. P. Schnyder, S. Ryu, A. Furusaki, and A. W. W. Ludwig, Phys. Rev. B **78**, 195125 (2008).
- [60] M. Sato, Y. Takahashi, and S. Fujimoto, Phys. Rev. Lett. **103**, 020401 (2009).
- [61] M. Sato, Y. Takahashi, and S. Fujimoto, Phys. Rev. B **82**, 134521 (2010).
- [62] P. Giannozzi, S. Baroni, N. Bonini, M. Calandra, *et al.*, Journal of Physics: Condensed Matter **21**, 395502 (2009).
- [63] P. Hohenberg and W. Kohn, Phys. Rev. **136**, B864 (1964).
- [64] W. Kohn and L. J. Sham, Phys. Rev. **140**, A1133 (1965).
- [65] D. Vanderbilt, Phys. Rev. B **41**, 7892 (1990).
- [66] C. J. Pickard, B. Winkler, R. K. Chen, M. C. Payne, M. H. Lee, J. S. Lin, J. A. White, V. Milman, and D. Vanderbilt, Phys. Rev. Lett. **85**, 5122 (2000).
- [67] J. P. Perdew, K. Burke, and M. Ernzerhof, Phys. Rev. Lett. **77**, 3865 (1996).